Chemical Engineering Journal 181–182 (2012) 72–79

Contents lists available at SciVerse ScienceDirect

Chemical Engineering Journal

journal homepage: www.elsevier.com/locate/cej

Adsorption capability for Congo red on nanocrystalline MFe_2O_4 (M = Mn, Fe, Co, Ni) spinel ferrites

Lixia Wang[a,b], Jianchen Li[a], Yingqi Wang[a], Lijun Zhao[a,*], Qing Jiang[a]

[a] Key Laboratory of Automobile Materials (Jilin University), Ministry of Education and School of Materials Science and Engineering, Jilin University, Changchun 130022, China
[b] School of Mechanical Science and Engineering, Northeast Petroleum University, Daqing 163318, China

ARTICLE INFO

Article history:
Received 19 September 2011
Received in revised form 26 October 2011
Accepted 26 October 2011

Keywords:
Ferrite
Adsorption
Desorption
Wastewater treatment
Congo red

ABSTRACT

In this contribution, we compare the adsorption capacity of different MFe_2O_4 (M = Mn, Fe, Co, Ni) ferrite nanocrystals synthesized by hydrothermal method for Congo red (CR). It is the first time to give a comprehensive comparison and analysis of the adsorption capacity of ferrite nanocrystals with spinel structure for CR. Research indicates that the cations distribution of MFe_2O_4 ferrites is the most important factor to decide their adsorption capacity. Electrostatic absorption was conceived as the main adsorption mechanism. Meanwhile, the MFe_2O_4 nanoparticles exhibited a clearly ferromagnetic behavior under applied magnetic field, which allowed their high-efficient magnetic separation from wastewater. Furthermore, acetone is an effective desorption agent for desorption of MFe_2O_4 nanoparticles loaded by CR. All of the spinel ferrite nanocrystals possess good soft-magnetism, especially, $CoFe_2O_4$ nanocrystals exhibit a higher saturation magnetization of 86.1 emu g^{-1} as well as the outstanding adsorption capacity for CR. By the calculation of Langmuir isotherm model, the maximum adsorption capacity of $CoFe_2O_4$ for CR is 244.5 mg g^{-1}.

1. Introduction

Dyes and pigments are widely used, mostly in the textiles, paper, plastics, leather, food and cosmetic industry to color products. The release of colored wastewater from these industries may present an eco toxic hazard. Such colored effluent can affect photosynthetic processes of aquatic plants, reducing oxygen levels in water and, in severe cases, resulting in the suffocation of aquatic flora and fauna. Most of the dyes, including Congo red, are toxic and must be removed before discharge into receiving streams since their effluents can reduce light penetration and photosynthesis [1].

The removal of dyes from aqueous environment has been widely studied and numerous methods such as coagulation [2], oxidation [3], photocatalysis [4], adsorption [5], nanofiltration [6], micellar enhanced ultrafiltration [7] etc, have been developed. Adsorption technology is currently being applied extensively to the removal of dyes from aqueous solutions. Several adsorbents have been investigated by previous researchers such as activated carbon [8], natural materials [5,9–11] and synthetic resins [12]. Widespread application of some of these adsorbents is restricted due to high cost, difficult disposal and regeneration. Furthermore, separation or recovery of these adsorbents in heterogeneous systems still remains a steep challenge. To overcome this engineering problem, various separation techniques such as free settling, centrifugation, and membrane filtration have been proposed over the years. Unfortunately, these separation techniques suffer from prolong usage of equipment operation, complicated technical requirements as well as high operational costs and thus severely restrict water treatment applications. Being an efficient and economical method, magnetic separation would be an ideal alternative than centrifugation or filtration methods. Nanosized magnetic particles are considered potential adsorbents for aqueous pollutants due to their high surface area and the unique advantage of easy separation under external magnetic fields. Several reports have been published on the using of various types of magnetic nanoparticles for removal, separation and determination of dyes [1,13–16] and metal ions [17–20]. In particular, the MFe_2O_4 (M = Mn, Fe, Co, Ni.) ferrites with spinel structure exhibit interesting magnetic, magnetoresistive, and magneto-optical properties that are potentially useful for a broad range of applications [21]. But it is a pity that there are very few studies about the Congo red (CR) removal by pure spinel ferrites, in fact, they also exhibit very good adsorption capacity for CR. By the comparative research about the adsorption capacity of the MFe_2O_4, the adsorption mechanism of MFe_2O_4 ferrites were disclosed.

* Corresponding author. Tel.: +86 431 85095878; fax: +86 431 85095876.
E-mail address: lijunzhao@jlu.edu.cn (L. Zhao).

1385-8947/$ – see front matter © 2011 Elsevier B.V. All rights reserved.
doi:10.1016/j.cej.2011.10.088

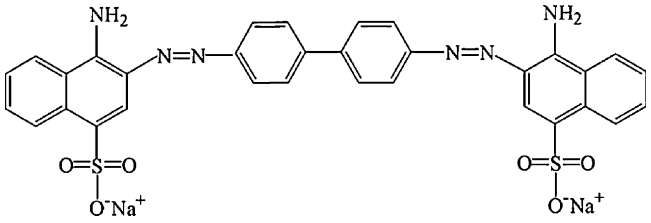

Scheme 1. Structure of CR molecule.

2. Materials and methods

2.1. Adsorbate

Congo red [CR, chemical formula = $C_{32}H_{22}N_6Na_2O_6S_2$, FW = 696.68, λ_{max} = 497 nm] is a benzidine-based anionic disazo dye, i.e. a dye with two azo groups. The structure is as illustrated in Scheme 1.

2.2. Synthesis of nanocrystalline MFe_2O_4

All chemicals were of analytical grade and were used without further purification. The chemicals were obtained from Beijing Chemicals Co. (Beijing, China).

In a typical experiment, $FeSO_4{\cdot}7H_2O$ or $FeCl_3{\cdot}6H_2O$ and MCl_2 (M = Mn, Co, Ni) were dissolved in 20 mL of distilled water by intensive stirring, accordingly a homogeneous solution was obtained, and then NaOH was added to the solution at room temperature with simultaneous vigorous agitation. The mixtures were stirred vigorously for 30 min, and then sealed in a Teflon-lined stainless-steel autoclave and maintained at 200 °C for 5 h. After the completion of the reaction, the solid product was collected by magnetic filtration and washed several times with deionized water and absolute ethanol respectively. The final product was dried in a vacuum oven at 100 °C for 6 h. Black powders were obtained and characterized as nanocrystalline MFe_2O_4 ferrites.

In order to obtain the Fe_3O_4 with smaller particle sizes, 0.200 g of $FeCl_3{\cdot}6H_2O$, 0.500 g of sodium citrate were dissolved in 20 mL of distilled water. Then 3.0 mL of ethylenediamine was added under continuous stirring until it was dissolved totally. The solution was transferred to a Teflon-lined autoclave. The autoclave was then sealed ad maintained at 200 °C for 12 h, other conditions were kept the same. Detailed experimental parameters are listed in Table 1 (from S1 to S5). Whole reaction preparing S1 and S4 was protected by Ar.

2.3. Characterization

The phases were identified by means of X-ray diffraction (XRD) with a Rigaku D/max 2500pc X-ray diffractometer with Cu Kα radiation (λ) 1.54156 Å at a scan rate of 0.02°/1(s), morphologies were characterized by a JEOL JSM-6700F field emission scanning electron microscopy (FESEM) operated at an acceleration voltage of 10.0 kV. The hysteresis loops were measured on a VSM-7300 vibrating sample magnetometer (VSM) (Lakeshore, USA) in room temperature. An Agilent Cary 50 UV–vis spectrophotometer was used for determination of CR concentration in the solutions.

2.4. Adsorption experiments

The stock solution of CR (1 g L^{-1}) was prepared in deionized water and desired concentrations of the dye were obtained by diluting the same with deionized water. The calibration curve of CR was prepared by measuring the absorbance of different predetermined concentrations of the samples at λ_{max} = 497 nm using UV–vis spectrophotometer (CR has a maximum absorbency at wavelength 497 nm on a UV–vis spectrophotometer). The amount of adsorbed CR (mg g^{-1}) was calculated based on a mass balance equation as given below:

$$q_e = \frac{(C_0 - C_e) \times V}{W} \quad (1)$$

where q_e is the equilibrium adsorption capacity per gram dry weight of the adsorbent, mg g^{-1}; C_0 is the initial concentration of CR in the solution, mg dm^{-3}; C_e is the final or equilibrium concentration of CR in the solution, mg dm^{-3}; V is the volume of the solution, dm^3; and W is the dry weight of the hydrogel beads, g.

Take one adsorption of CR for example. Standard solution with initial concentrations of 100 mg L^{-1} was prepared. Then, 15 mg of MFe_2O_4 nanoparticles was added to 50 mL of above solution under stirring. After a specified time, the solid and liquid were separated by magnet and UV–vis adsorption spectra was used to measure the CR concentration in the remaining solutions. A standard curve, which was used to convert absorbance data into concentrations for kinetic and equilibrium studies, was drawn to calculate the concentration of each experiment.

3. Results and discussion

3.1. Characterization of nanocrystalline MFe_2O_4 (M = Mn, Fe, Co, Ni) ferrites

The FESEM image (Fig. 1a) shows that the product S1 consists of irregular polyhedral, their edge lengths are in the range of 50–400 nm. Uniform nanoparticles with particle sizes around 25 nm are observed from Fig. 1b. In Fig. 1c, we can observe large numbers of octahedral with some small nanoparticles adsorbed on their surfaces. The lateral sizes of octahedral are ranging from 80 to 100 nm and the nanoparticles with about 10–20 nm in diameters. S4 and S5 are composed by octahedral nanoparticles, their particle sizes are in the range of 80–100 nm and 30–40 nm, respectively.

Fig. 1f shows the XRD patterns of S1–S5. All the diffraction peaks of S1 and S2 can be indexed to the face-centered cubic structure of magnetite according to JCPDS card No. 19-0629. The diffraction peaks for S5 (Fig. 1f b)) can be indexed to face center cubic structure of cobalt ferrite according to JCPDS card No. 22-1086. For S4 (Fig. 1f c)), the peak can be indexed to face center cubic structure of

Table 1
Summary of the experimental parameters.

Samples	Iron source (g)		Salt (g)	Additives (g)	Alkali		Ar	Reaction times (h)
	$FeSO_4{\cdot}7H_2O$	$FeCl_3{\cdot}6H_2O$			NaOH (g)	EDA (mL)		
S1 (Fe_3O_4)	0.834	–	–	–	1.5	–	With	5
S2 (Fe_3O_4)	–	0.200	–	Citric acid (0.5)	–	3.0	Without	12
S3 ($NiFe_2O_4$)	–	0.541	$NiCl_2{\cdot}6H_2O$ (0.238)	–	1.5	–	Without	5
S4 ($MnFe_2O_4$)	0.556	–	$MnCl_2{\cdot}4H_2O$(0.198)	–	1.5	–	With	5
S5 ($CoFe_2O_4$)	0.556	–	$CoCl_2{\cdot}6H_2O$ (0.238)	–	1.5	–	Without	5

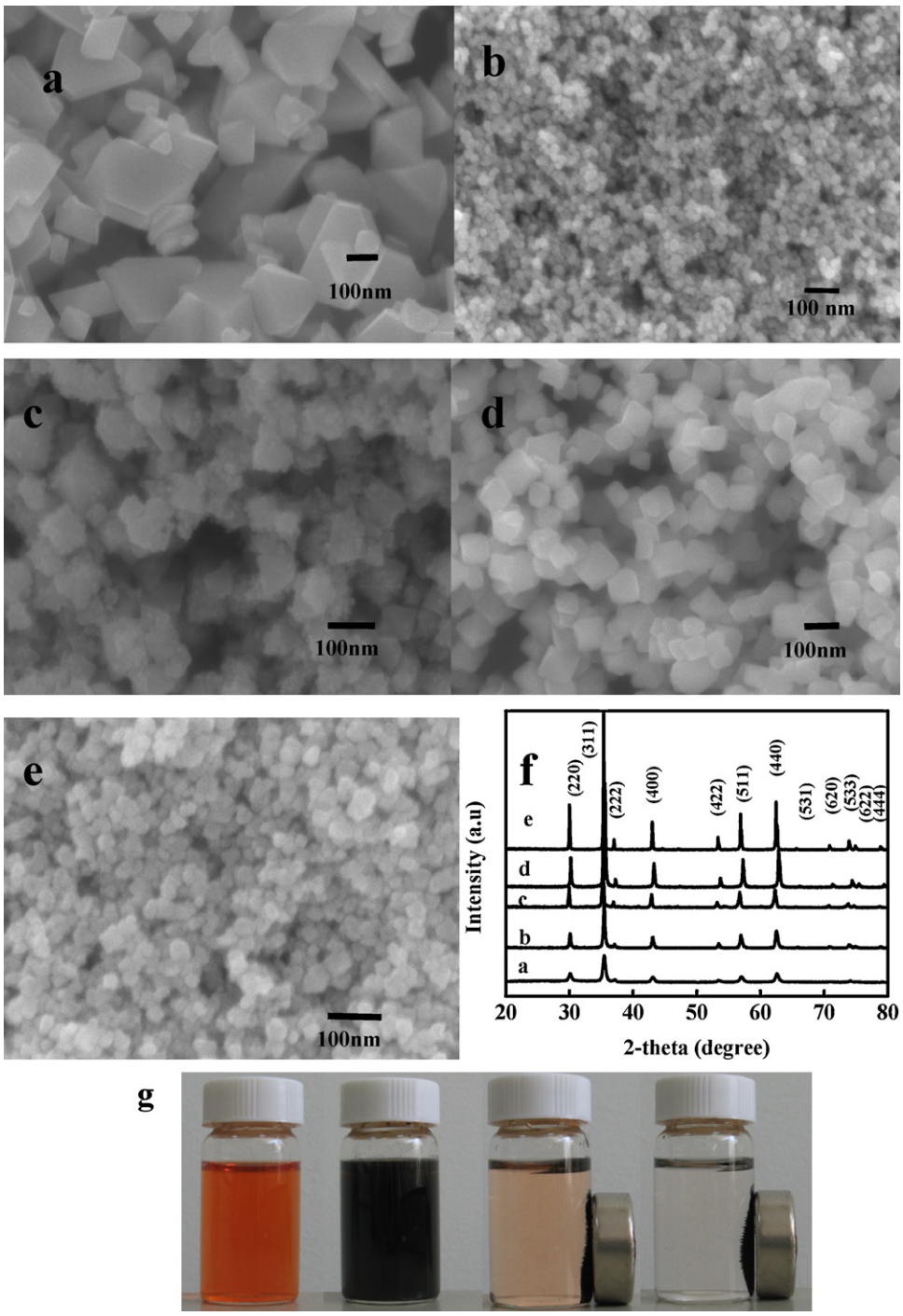

Fig. 1. SEM images of (a) S1, (b) S2, (c) S3, (d) S4 and (e) S5; (f) XRD patterns of: a) S2, b) S5, c) S4, d) S3 and e) S1; (g) adsorption process of MFe_2O_4 in different times: CR solution; for 2 min; for 40 min.

jacobsite ferrite (JCPDS No. 10-0319). The diffraction peaks for S3 (Fig. 1f d)) can be indexed to face center cubic structure of nickel ferrite according to JCPDS card No. 10-0325. The sharpness of the X-ray diffraction peaks confirms that the material should be highly crystallized MFe_2O_4 without any other impurities.

3.2. Effects of initial CR concentration

After we ascertain the pure phase MFe_2O_4 spinel ferrites, a series adsorption experiments were carried out. Effect of the concentration of CR was investigated by repeating experiments with different initial concentrations (50, 75, 100, 125 and 150 mg L^{-1}) of CR. Fig. 2(a–e) reveals the dependence of adsorption capacities of $MnFe_2O_4$ for CR on their concentrations. When the initial CR concentration varied from 50 to 150 mg L^{-1}, the adsorption capacity of S1–S5 increased from 16.7 to 30.6 mg g^{-1}, 63.1 to 87.5 mg g^{-1}, 50.2 to 71.3 mg g^{-1}, 35.5 to 68.0 mg g^{-1} and 82.6 to 170.0 mg g^{-1}, respectively. Fig. 2 also indicates that the adsorption of CR is fast at the initial stage, and then, it becomes slower near the equilibrium. It would be for that a large number of vacant surface sites are available for adsorption during the initial stage of the treatment time, and after a lapse of time, the remaining vacant surface sites are

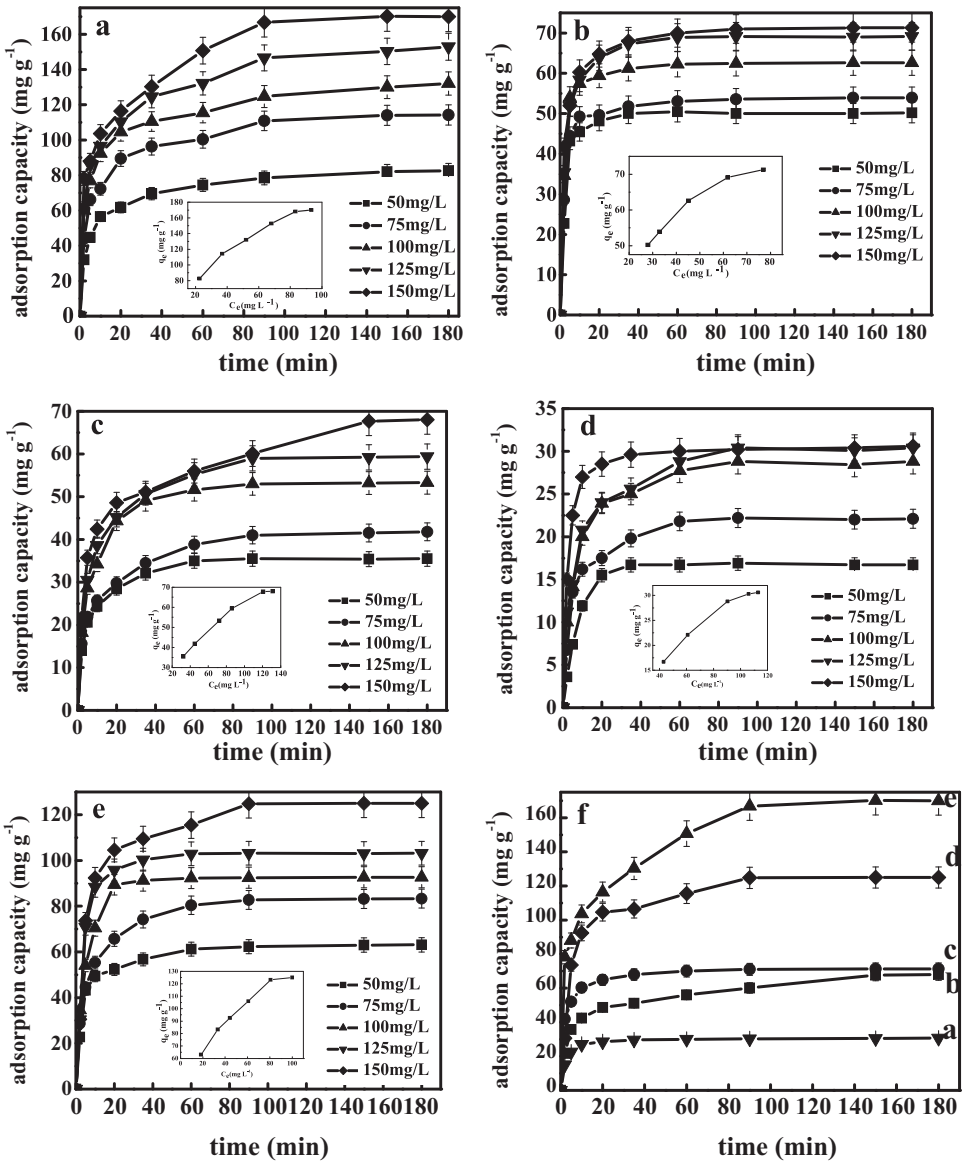

Fig. 2. Effect of initial dye concentration on CR removal: (a) S5, (b) S3, (c) S4, (d) S1 and (e) S2; (f) adsorption capacity of: a) S1, b) S4, c) S3, d) S2 and e) S5. (Adsorption conditions for CR: 50 mL of 150 mg L^{-1} of dye, adsorbent dosage 0.015 g, natural pH, temperature: 18 °C).

difficult to be occupied due to repulsive forces between CR adsorbed on the surface of MFe_2O_4 ferrites and solution phase. It is clear that the adsorption process is highly dependent on initial concentration of solution. Similar results have been reported for the adsorption of CR on Ca-bentonite in work done by Lian et al. [22].

The adsorption capacity of S1–S5 for CR was shown in Fig. 2f. Aqueous solutions with initial CR concentration 150 mg L^{-1} was used for the experiment at neutral pH 7, adsorption different time from 0 to 180 min, and T = 18 °C. The equilibrium adsorption capacity of S1–S5 for CR are 30.6,87.5,71.3, 68.0 and 170.0 mg g^{-1}, respectively. $CoFe_2O_4$ (S5) exhibits the highest adsorption capacity among theses spinel ferrites. Saturation adsorption capacities of S5 for CR are over five times than that of S1.

Fig. 1f shows the adsorption process of MFe_2O_4 in different times. A light pink solution was observed after 2 min of adsorption. Further prolonging the adsorption time to 40 min, a colorless solution was gained. More importantly, simple and rapid separation of CR-loaded MFe_2O_4 adsorbent from treated water can be achieved via an external magnetic field.

3.3. Adsorption isotherms

The adsorption isotherm of a specific adsorbent represents its adsorptive characteristics and is very important to the design of adsorption processes. To simulate the adsorption isotherm, two commonly used models, the Langmuir [23] (Eq. (2)) and Freundlich [24] (Eq. (3)) isotherms, were selected to explicate dye–ferrite interaction.

$$\frac{1}{q_e} = \frac{1}{q_{max}} + \frac{1}{K_L q_{max}} \frac{1}{C_e} \quad (2)$$

$$\log q_e = \log K_F + \frac{1}{n} \log C_e \quad (3)$$

where q_{max} is the maximum amount of adsorption with complete monolayer coverage on the adsorbent surface (mg g^{-1}), and K_L is the Langmuir constant related to the energy of adsorption (L mg^{-1}). The Langmuir constants K_L and q_{max} can be determined from the linear plot of $1/C_e$ versus $1/q_e$. K_F and n are the Freundlich adsorption isotherm constants, being indicative of the extent of the adsorption and the degree of nonlinearity between solution

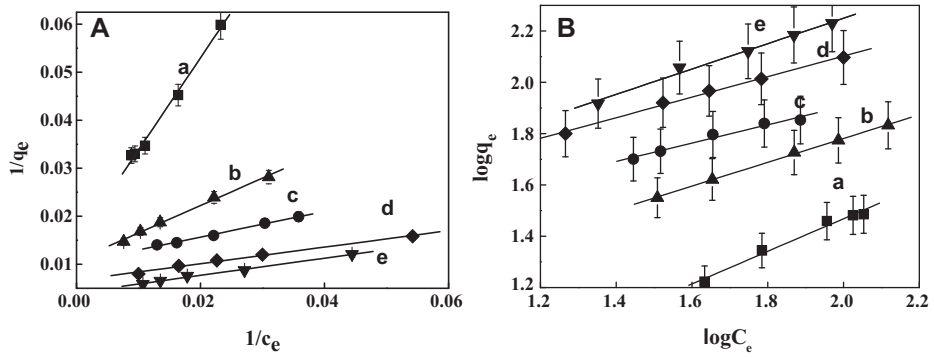

Fig. 3. Adsorption isotherm for adsorption of CR: (A) Langmuir and (B) Freundlich of (a) S1, (b) S4, (c) S3, (d) S2 and (e) S5.

concentration and adsorption, respectively. K_F and $1/n$ values can be calculated from intercept and slope of the linear plot between $\log C_e$ and $\log q_e$.

The Freundlich isotherm was employed to describe heterogeneous systems and reversible adsorption, which does not restrict to the monolayer formations. Unlike the Freundlich isotherm, the Langmuir isotherm is based on the assumption that a structure of adsorbent is homogeneous, where all sorption sites are identical and energetically equivalent.

Inset in Fig. 2(a–e) show their equilibrium adsorption curves of CR on spinel ferrites at room temperature. It can be seen that at lower adsorption equilibrium dye concentration, adsorption capacity rises sharply and thereafter the increase is gradual with an increase of equilibrium dye concentration. Fig. 3 represents the plot of the experimental data based on Langmuir and Freundlich isotherms model, respectively. Table 2 shows the calculated values of Langmuir and Freundlich model's parameters. The comparison of correlation coefficients (r^2) of the linearized form of both equations indicates and non-linear isothermal scatters that the Langmuir model yields a better fit for the experimental equilibrium adsorption data than the Freundlich model. The maximum adsorption capacity of S1–S5 for CR calculated from the Langmuir isotherm model are 68.5, 149.7, 97.1, 92.4 and 244.5 mg g^{-1}, respectively, as shown in Table 2.

The essential characteristics of Langmuir isotherm can be expressed by a dimensionless constant called equilibrium parameter R_L that is defined by the following equation:

$$R_L = \frac{1}{(1 + K_L C_0)} \tag{4}$$

where K_L and C_0 are the same as defined before. The value of R_L calculated from the above expression. The nature of the adsorption process to be either unfavourable ($R_L > 1$), linear ($R_L = 1$), favourable ($0 < R_L < 1$) or irreversible ($R_L = 0$). Here, R_L-values obtained are listed in Table 2. All the R_L-values for the adsorption of CR onto MFe_2O_4 NPs are in the range of 0–1, indicating that the adsorption process is favourable.

3.4. Adsorption kinetics

The adsorption kinetic models were applied to interpret the experimental data to determine the controlling mechanism of dye adsorptions from aqueous solution. Here, Pseudo-first-order, pseudo-second-order and the intraparticle diffusion model were used to test dynamical experimental data.

The pseudo-first-order kinetic model of Lagergren [25] is given by:

$$\log(q_{1e} - q_t) = \log q_{1e} - \frac{K_1 t}{2.303} \tag{5}$$

where q_t is the amount of dye adsorbed per unit of adsorbent (mg g^{-1}) at time t, K_1 is the pseudo-first-order rate constant (min^{-1}). The adsorption rate constant (K_1) were calculated from the plot of $\log(q_{1e} - q_t)$ against t.

Ho and McKay [26] presented the pseudo-second-order kinetic as:

$$\frac{1}{q_t} = \frac{1}{K_2 q_{2e^2}} + \frac{1}{q_{2e}} \tag{6}$$

where K_2 is the pseudo-second-order rate constant (g mg^{-1} min^{-1}). The initial adsorption rate, h (mg g^{-1} min^{-1}) at $t \to 0$ is defined as:

$$h = K_2 q_{2e^2} \tag{7}$$

The h, q_{2e} and K_2 can be obtained by linear plot of t/q_t versus t.

Fig. 4 is the plots of the pseudo-first-order and second order kinetics of CR adsorption on MFe_2O_4. The calculated kinetic parameters are given in Table 3. The comparison of correlation coefficients (r^2) of both models result suggests that the adsorption process does not follow the pseudo-first-order kinetic model, on the contrary, the results present an ideal fit to the second order kinetic for adsorbent. A good agreement with this adsorption model is confirmed by the similar values of calculated q_{2e} and the experimental ones for adsorbent. The best fit to the pseudo-second-order kinetics indicates that the adsorption mechanism depends on the adsorbate and adsorbent.

Table 2
Adsorption isothermal constants calculated from Langmuir and Freundlich models.

Samples	Langmuir model					Freundlich model			
	q_{max} (mg g^{-1})	K_L (L mg^{-1})	r_L^2	R_L	SD	K_F ($mg^{1-1/n}$ $L^{1/n}$ g^{-1})	n	r_F^2	SD
S1	68.5	0.0076	0.9933	0–1	0.0011	1.57	1.57	0.9815	0.0179
S2	149.7	0.0387	0.9958	0–1	3.1E−4	20.04	2.50	0.9882	0.0100
S3	97.1	0.0385	0.9938	0–1	2.3E−4	15.52	2.80	0.9737	0.0124
S4	92.4	0.0190	0.9950	0–1	4.5E−4	7.14	2.16	0.9989	0.0044
S5	244.5	0.0228	0.9944	0–1	2.1E−4	18.26	2.02	0.9887	0.0150

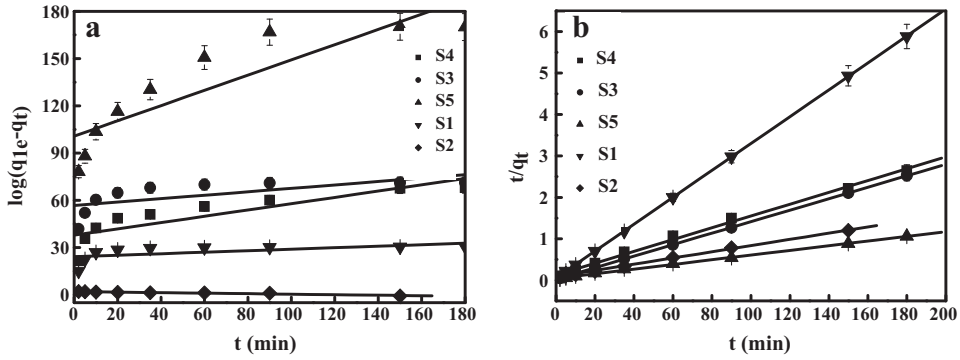

Fig. 4. Adsorption kinetic for adsorption of CR on MFe_2O_4 (initial dye concentration 150 mg L^{-1}, natural pH, temperature: 18 °C). (a) Pseudo-first-order and (b) Pseudo-second-order.

Table 3
Adsorption parameters got from kinetic for the adsorption of 150 mg L^{-1} CR on MFe_2O_4.

Samples	$q_{e,exp}$ (mg g^{-1})	Pseudo-first-order				Pseudo-second-order				
		K_1 (min^{-1})	q_{1e} (mg g^{-1})	r_1^2	SD	K_2 (g mg^{-1} min^{-1})	q_{2e} (mg g^{-1})	h (mg g^{-1} min^{-1})	r_2^2	SD
S1	30.7	0.026	5.46	0.8017	0.3156	0.0187	30.8	17.78	1.0000	0.0100
S2	125.0	0.038	105.60	0.9326	0.2463	0.0006	133.3	11.54	0.9960	0.026
S3	71.3	0.049	22.14	0.9793	0.1101	0.0074	72.2	38.45	1.0000	0.0043
S4	68.0	0.029	45.68	0.9112	0.2211	0.0016	70.2	7.95	0.9954	0.0677
S5	170.2	0.035	107.31	0.9894	0.1024	0.0008	177.0	23.75	0.9976	0.0191

3.5. Adsorption thermodynamics

Thermodynamic parameter related to the adsorption process i.e., free energy change (ΔG, kJ mol^{-1}) for adsorption was calculated using the following equation [27]:

$$\Delta G = -RT\ln K_c \quad (8)$$

where R is the universal gas constant (8.314 J mol^{-1} K^{-1}), T is the temperature (K) and K_c is equilibrium constant. The K_c value is calculated from Eq. (9):

$$K_c = \frac{C_{AE}}{C_{SE}} \quad (9)$$

where K_c is the adsorption equilibrium constant. C_{AE} is the amount of dye (mg) adsorbed on the adsorbent per litre of the solution at equilibrium. C_{SE} is the equilibrium concentration (mg L^{-1}) of the dye in the solution. The calculated ΔG values obtained are given in Table 4 at T = 18 °C. The negative value of free energy change indicated the spontaneous nature of sorption and confirmed affinity of adsorbent for the dyes [22,28].

3.6. Why do the MFe_2O_4 ferrites with the same spinel structure show different adsorption capacity?

Based on the adsorption kinetics, thermodynamics and experimental results, we inferred that electro-static absorption was the main adsorption mechanism. Discussing the source of charges on the ferrite surfaces may be more useful before investigating the change of zeta potential with equilibrium pH of adsorbent in electrolyte media. Below the pH_{IEP} (the pH of zero point charge), the adsorbent surface is positive charge, and anion adsorption occurs.

Table 4
Thermodynamic parameters for the adsorption of CR onto spinel ferrites.

Samples	S1	S2	S3	S4	S5
K_c	5.29	26.96	26.82	13.23	15.88
ΔG (kJ mol^{-1})	−4.03	−7.97	−7.96	−6.25	−6.69

Otherwise, it would show negative charges, so that the extent of adsorption of cationic dyes is increased. The pH_{IEP} of MFe_2O_4 (M = Mn, Fe, Co, Ni) are 4.5 [29], 6.5 [30], 6.5–6.6 [30,31] and 6.6–6.8 [32], respectively. Through the reliability evaluation of pH value about the CR solution by pH meter, the final pH value was estimated at 7.0. The actual pH value is larger than all of the pH_{IEP} value of ferrites, so the adsorbent surfaces have negative charges. There are two functional groups in Congo red molecules, i.e. sulfonic acid group and amine group. The sulfonic acid and amine group can be completely dissolved and protonated in water, thus become negative charged and positive charged in water, respectively. There are two primary amino groups (–NH_2) attached to the two naphthalene rings located at the two ends of the CR molecule, respectively. Furthermore, –NH_2 is both the hydrophilic and chromogenic group. Hence, the existence of –NH_2 makes CR dissolve into the water and show red color in the water. The ferrites with negative charges are prone to adsorb the protonated –NH_2 which shows positive charges, accordingly the CR are adsorbed on the surface of ferrite. At last, the clear solution was obtained after the electrostatic interaction between the ferrite and CR.

For S1 and S4, their adsorption values for CR are the lowest. It may be because of the flow of Ar gas during the preparation process. Ar gas flow during the synthetic process can influence the adsorption of electric charge on particle surface; therefore, the adsorption capacities for S1 and S4 are lower than other samples. Furthermore, the particle sizes of S4 are lower than those of S1, and the cations distribution for S1 and S4 are different, so the adsorption capacity of S4 are higher than that of S1. Fe_3O_4 and $NiFe_2O_4$ are the typical inverse spinel ferrites; whereas, the $MnFe_2O_4$ and $CoFe_2O_4$ are the mixed spinel ferrites. The cations distribution for AB_2O_4 ferrite are illustrated as: $Fe^{3+}[Fe^{2+}Fe^{3+}]O_4$, $Fe^{3+}[Ni^{2+}Fe^{3+}]O_4$, $Fe^{3+}Mn_x{}^{2+}[Mn_{1-x}{}^{2+}Fe^{3+}]O_4$ and $Fe^{3+}Co^{2+}{}_x[Co_{1-x}{}^{2+}Fe^{3+}]O_4$. It is well known that the structural formula of Fe_3O_4 also can be written as $FeO{\cdot}Fe_2O_3$. Hence, we can believe that other spinel ferrites are the forms of substitution of Fe^{2+} ions in the FeO by specific bivalent metal ions (Mn^{2+}, Co^{2+}, Ni^{2+}). To $NiFe_2O_4$ ferrite, it has inverse spinel structure as Fe_3O_4, and $\gamma_{Ni^{2+}}$ is close to $\gamma_{Fe^{2+}}$ ($\gamma_{Ni^{2+}} = 0.69\,Å$, $\gamma_{Fe^{2+}} = 0.74\,Å$). If they

Table 5
Desorption efficiency in alcohol and acetone.

Reagent	S1 (%)	S2 (%)	S3 (%)	S4 (%)	S5 (%)
Alcohol	56.0	48.0	54.0	52.0	49.0
Acetone	88.0	76.0	87.0	85.0	79.0

have similar particle size, $NiFe_2O_4$ and Fe_3O_4 should show alike adsorption capacity. But the particle size of S3 is larger than that of S2, obviously, the adsorption capacity of S3 is a little weaker than that of S2. Compared with Fe_3O_4, the A-sites are distorted to some extent because of $\gamma_{Co^{2+}} > \gamma_{Fe^{3+}}$ ($\gamma_{Co^{2+}} = 0.72\,Å$, $\gamma_{Fe^{3+}} = 0.56\,Å$), which may cause the increase of the adsorption charge on the surface of $CoFe_2O_4$. Thereby, the adsorption capacity of $CoFe_2O_4$ is higher than that of Fe_3O_4. In summary, the cations distribution of spinel ferrites may be the most important factor to decide their adsorption capacity.

3.7. Desorption

The use of an adsorbent in the wastewater treatment depends not only on the adsorptive capacity, but also on how well the adsorbent can be regenerated and used again. For repeated use of an adsorbent, adsorbed dye should be easily desorbed under suitable conditions. Desorption process was conducted by mixing 5 mg of CR-loaded modified MFe_2O_4 with 30 mL of acetone solutions or alcohol and shaking for 30 min. The desorption efficiency calculated as:

$$\text{Desorption ratio (\%)} = \frac{\text{amount of desorbed CR}}{\text{amount of adsorbed CR}} \times 100 \qquad (10)$$

The calculated desorption efficiency are given in Table 5. Therefore, the CR could be desorbed from the loaded nanoparticles by acetone solutions.

3.8. Performance evaluation

The maximum adsorption capacity (q_{max}) of S1–S5 nanoparticles for CR calculated from the Langmuir isotherm model are listed in Table 6 with literature values of q_{max} of other adsorbents for CR adsorption [33–35,11,36,37]. Except for Fe_3O_4@meso C nanocapsules, the MFe_2O_4 ferrites used in this study possess have considerable higher q_{max} values. However, the simplicity of the preparation method and magnetic separation makes MFe_2O_4 ferrites better adsorbent for CR.

3.9. Magnetic properties

The magnetic properties of magnetic absorbents directly influence the callback efficiency. Hence, excellent magnetic performance is also a key role for the magnetic material as magnetic absorbent. Magnetic properties of the as-synthesized MFe_2O_4 nanocrystalline were measured at room temperature, and five samples showed a typical hysteresis loop in their magnetic behavior, as observed in Fig. 5. The insets are magnified views of the hysteresis loops at low applied fields. Furthermore, the magnetic parameters of samples obtained from hysteresis loops were listed in Table 7. The MFe_2O_4 ferrites with high saturation magnetization values can quickly respond to the external magnetic field, which is beneficial to their application in high-capacity adsorption. Especially, $CoFe_2O_4$ nanocrystals exhibit a higher saturation magnetization of 86.1 emu g^{-1} as well as the outstanding adsorption capacity for CR. The as-obtained MFe_2O_4 ferrites with excellent soft-magnetism can be used as a reusable absorbent for fast, convenient, and highly efficient removal of dyes from the wastewater.

Table 6
Adsorption capacities of CR dye on various adsorbents.

Type of adsorbent	q_{max} (mg g^{-1})	Reference
$CoFe_2O_4$ (S5)	244.5	Present study
Fe_3O_4 (S2)	149.7	Present study
$NiFe_2O_4$ (S3)	97.1	Present study
$MnFe_2O_4$ (S4)	92.4	Present study
Fe_3O_4 (S1)	68.5	Present study
Maghemite nanoparticles	208.3	[33]
Magnetic core–manganese oxide shell nanoparticles	42.0	[34]
Fe_3O_4@meso C nanocapsules	1656.9	[35]
Rice bran	14.6	[11]
Bentonite	19.9	[36]
Activated carbon prepared from coir pith	6.7	[37]

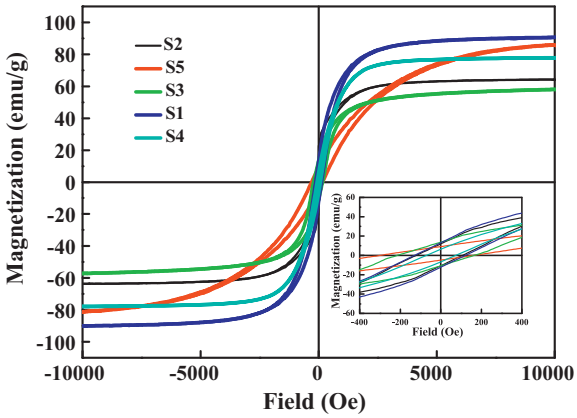

Fig. 5. Magnetization curve measured at room temperature for the spinel ferrites.

Table 7
Magnetic parameters of MFe_2O_4 nanocrystalline at room temperature.

Samples	Ms (emu g^{-1})	Mr (emu g^{-1})	Hc (Oe)
S1 (Fe_3O_4)	90.8	13.9	124.7
S2 (Fe_3O_4)	64.8	11.9	104.6
S3 ($NiFe_2O_4$)	58.0	13.6	166.7
S4 ($MnFe_2O_4$)	78.4	6.6	76.4
S5 ($CoFe_2O_4$)	86.1	9.4	162.3

4. Conclusions

Nanocrystalline MFe_2O_4 ferrites with spinel structure were successfully synthesized by a facile one-step hydrothermal synthesis. The maximum adsorption capacity of S1– S5 for CR calculated from the Langmuir isotherm model are 68.5, 149.7, 97.1, 92.4 and 244.5 mg g^{-1}, respectively. Factors affecting adsorption, such as, initial dye concentration and contact time were evaluated. The desorption efficiency of S1–S5 in acetone solutions calculated are 88.0, 76.0, 87.0, 85.0 and 79.0%, respectively. Furthermore, analysis of adsorption isotherm shows that our adsorption experiment accord with Langmuir model. Adsorption kinetics indicates that the adsorption mechanism depends on the adsorbate and adsorbent. Thermodynamic study showed that the adsorption processes are spontaneous. We draw an important conclusion by our experimental data that adsorption capacity of MFe_2O_4 ferrites is influenced by the cations distribution on the A- and B-sites. By integrated analysis and comparison, $CoFe_2O_4$ nanocrystals are the most excellent candidate among these ferrites for possible application in the field of water treatment.

Acknowledgement

The financial supports from the Natural Science Foundation of Jilin Province (20101542) of China and the National Foundation of Doctoral Station (grant no. 20100061110019) are acknowledged.

References

[1] M. Iram, C. Guo, Y. Guan, A. Ishfaq, H. Liu, Adsorption and magnetic removal of neutral red dye from aqueous solution using Fe_3O_4 hollow nanospheres, J. Hazard. Mater. 181 (2010) 1039–1050.
[2] M.L. Marechal, Y.M. Slokar, T. Taufer, Decolouration of chlorotriazine reactive azo dyes with H_2O_2/UV, Dyes Pigments 33 (1997) 181–298.
[3] W.X. Chen, W.Y. Lu, Y.Y. Yao, M.H. Xu, Highly efficient decomposition of organic dyes by aqueous-fiber phase transfer and in situ catalytic oxidation using fiber-supported cobalt phthalocyanine, Environ. Sci. Technol. 41 (2007) 6240–6245.
[4] J. Fernandez, J. Kiwi, C. Lizama, J. Freer, J. Baeza, H.D. Mansilla, Factorial experimental design of orange II photocatalytic discoloration process, J. Photochem. Photobiol. A 151 (2002) 213–219.
[5] M. Arami, N.Y. Limaee, N.M. Mahmoodi, N.S. Tabrizi, Removal of dyes from colored textile wastewater by orange peel adsorbent: equilibrium and kinetic studies, J. Colloid Interface Sci. 288 (2005) 371–376.
[6] S. Chakraborty, M.K. Purkait, S. Dasgupta, S. De, J.K. Basu, Nanofiltration of textile plant effluent for color removal and reduction in COD, Sep. Purif. Technol. 31 (2003) 141–151.
[7] M.K. Purkait, S. DasGupta, S. De, Removal of dye from wastewater using micellar-enhanced ultrafiltration and recovery of surfactant, Sep. Purif. Technol. 37 (2004) 81–92.
[8] M.K. Purkait, A. Maiti, S. DasGupta, S. De, Removal of Congo red using activated carbon and its regeneration, J. Hazard. Mater. 145 (2007) 287–295.
[9] R. Jain, S. Sikarwar, Removal of hazardous dye Congo red from waste material, J. Hazard. Mater. 152 (2008) 942–948.
[10] Z. Yermiyahu, I. Lapides, S. Yariv, Visible absorption spectroscopy study of the adsorption of Congo Red by montmorillonite, Clay Miner. 38 (2003) 483–500.
[11] X.S. Wang, J.P. Chen, Biosorption of Congo Red from aqueous solution using Wheat Bran and Rice Bran: batch studies, Sep. Sci. Technol. 44 (2009) 1452–1466.
[12] Y. Yu, Y.Y. Zhuang, Z.H. Wang, M.Q. Qiu, Adsorption of water-soluble dyes onto Resin NKZ, Ind. Eng. Chem. Res. 42 (2003) 6898–6903.
[13] X.Y. Hou, J. Feng, X.H. Liu, Y.M. Ren, Z.J. Fan, M.L. Zhang, Magnetic and high rate adsorption properties of porous $Mn_{1-x}Zn_xFe_2O_4$ ($0 \leq x \leq 0.8$) adsorbents, J. Colloid Interface Sci. 353 (2011) 524–529.
[14] L. Ai, Y. Zhou, J. Jiang, Removal of methylene blue from aqueous solution by montmorillonite/$CoFe_2O_4$ composite with magnetic separation performance, Desalination 266 (2011) 72–77.
[15] L. Zhou, C. Gao, W. Xu, Magnetic dendritic materials for highly efficient adsorption of dyes and drugs, ACS Appl. Mater. Interface 2 (2010) 1483–1491.
[16] B. Zargar, H. Parham, A. Hatamie, Fast removal and recovery of amaranth by modified iron oxide magnetic nanoparticles, Chemosphere 76 (2009) 554–557.
[17] S.X. Zhang, H.Y. Niu, Y.Q. Cai, X. Zhao, Y.L. Shi, Arsenite and arsenate adsorption on coprecipitated bimetal oxide magnetic nanomaterials: $MnFe_2O_4$ and $CoFe_2O_4$, Chem. Eng. J. 158 (2010) 599–607.
[18] T. Zhang, X. Zhang, H. Yang, J.C. Liu, D.D. Sun, Fabrication of magnetic cryptomelane-type manganese oxide nanowires for water treatment, Chem. Commun. 47 (2011) 1890–1892.
[19] L.S. Zhong, J.S. Hu, H.P. Liang, A.M. Cao, W.G. Song, L.J. Wan, Self-assembled 3D flowerlike iron oxide nanostructures and their application in water treatment, Adv. Mater. 18 (2006) 2426–2431.
[20] P. Panneerselvam, N. Morad, K.A. Tan, Magnetic nanoparticle (Fe_3O_4) impregnated onto tea waste for the removal of nickel(II) from aqueous solution, J. Hazard. Mater. 186 (2011) 160–168.
[21] N. Bao, L. Shen, Y. Wang, P. Padhan, A. Gupta, A facile thermolysis route to monodisperse ferrite nanocrystals, J. Am. Chem. Soc. 129 (2007) 12374–12375.
[22] L. Lian, L. Guo, C. Guo, Adsorption of Congo red from aqueous solutions onto Ca-bentonite, J. Hazard. Mater. 161 (2009) 126–131.
[23] I. Langmuir, The adsorption of gases on plane surfaces of glass, mica and platinum, J. Am. Chem. Soc. 40 (1918) 1361–1403.
[24] H.M.F. Freundlich, Uber die adsorption in losungen, Z. Phys. Chem. 57 (1906) 385–470.
[25] S. Lagergren, About the theory of so-called adsorption of soluble substances, Kungliga Svenska Vetenskapsakademiens Handlingar 24 (1898) 1–39.
[26] Y.S. Ho, G. McKay, Pseudo-second order model for sorption processes, Process Biochem. 34 (1999) 451–465.
[27] W. Stumm, J.J. Morgan, Aquatic Chemistry: Chemical Equilibrium and Rates in Natural Waters, 3rd ed., Wiley, New York, 1995, p. 1040.
[28] B. Acemioğlu, Adsorption of Congo red from aqueous solution onto calcium-rich fly ash, J. Colloid Interface Sci. 274 (2004) 371–379.
[29] M.L. Esteves, A. Cortes, M.T. Lugo, C. Rinaldi, Synthesis and characterization of carboxymethyl dextran-coated Mn/Zn ferrite for biomedical applications, J. Magn. Magn. Mater. 321 (2009) 3061–3066.
[30] M. Barale, G. Lefèvre, F. Carrette, H. Catalette, M. Fédoroff, G. Cote, Effect of the adsorption of lithium and borate species on the zeta potential of particles of cobalt ferrite, nickel ferrite, and magnetite, J. Colloid Interface Sci. 328 (2008) 34–40.
[31] J. Vicente, J.D.G. Duraĭn, A.V. Delgado, Electrokinetic and viscoelastic properties of magnetorheological suspensions of cobalt ferrite, Colloid Surf. A. 195 (2001) 181–188.
[32] R.C. Plaza, J. de Vicente, S. Gĭomez-Lopera, A.V. Delgado, Stability of dispersions of colloidal nickel ferrite spheres, J. Colloid Interface Sci. 242 (2001) 306–313.
[33] A. Afkhami, R. Moosavi, Adsorptive removal of Congo red, a carcinogenic textile dye, from aqueous solutions by maghemite nanoparticles, J. Hazard. Mater. 174 (2010) 398–403.
[34] Y. Zhai, J.F. Zhai, M. Zhou, S.J. Dong, Ordered magnetic core–manganese oxide shell nanostructures and their application in water treatment, J. Mater. Chem. 19 (2009) 7030–7035.
[35] Y.X. Zhang, S.C. Xu, Y. Luo, S. Pan, H. Ding, G.H. Li, Synthesis of mesoporous carbon capsules encapsulated with magnetite nanoparticles and their application in wastewater treatment, J. Mater. Chem. 21 (2011) 3664–3671.
[36] G.C. Panda1, S.K. Das1, A.K. Guha, Jute stick powder as a potential biomass for the removal of Congo red and rhodamine B from their aqueous solution, J. Hazard. Mater. 164 (2009) 374–379.
[37] C. Namasivayam, D. Kavitha, Removal of Congo Red from water by adsorption onto activated carbon prepared from coir pith, an agricultural solid waste, Dyes Pigments 54 (2002) 47–58.